Full Articles

Features of the decomposition of the nitrosyl iron complex with thiourea ligands under aerobic conditions: experiment and kinetic and quantum chemical modeling*

O. V. Pokidova,[a]★ B. L. Psikha,[a] N. S. Emel'yanova,[a,b] L. G. Gutsev,[a] V. O. Novikova,[a] E. A. Zagainova,[a,b] and N. A. Sanina[a,b,c]

[a] Institute of Problems of Chemical Physics, Russian Academy of Sciences, 1 prosp. Akad. Semenova, 142432 Chernogolovka, Moscow Region, Russian Federation. Fax: +7 (496) 522 3507. E-mail: pov@icp.ac.ru
[b] Faculty of Fundamental Physical and Chemical Engineering, Lomonosov Moscow State University, Build. 51, 1 Leninskie Gory, 119991 Moscow, Russian Federation
[c] Scientific and Educational Center "Medical Chemistry" of the Moscow State Regional University, 24 ul. Very Voloshinoi, 141014 Mytishchi, Moscow Region, Russian Federation

The reaction of oxygen with the nitrosyl iron complex $[Fe(SC(NH_2)_2)_2(NO)_2]^+$ (complex **1**) was studied. According to the results obtained, three main directions of transformation of complex **1** under aerobic conditions can be distinguished: (i) reversible binding of complex **1** with oxygen leading to a sharp decrease in the oxygen concentration at the initial moment, (ii) irreversible spontaneous transformation of complex **1** without participation of oxygen accompanied by the elimination of thio ligands and NO groups, and (iii) irreversible reaction of complex **1** with oxygen to form oxygen coordination products (at the iron atom, Fe—N bond, and two N atoms of nitrosyl ligands), which then reversibly transform into oxidation products. The latter process is accompanied by an increase in the absorbance in the experimental UV spectra and the formation of nitrates and nitrites in the reaction system.

Key words: reaction rate constant, nitrosyl iron complexes, nitric oxide, NO donor, kinetic modeling, quantum chemical modeling, UV spectroscopy.

* Dedicated to Academician of the Russian Academy of Sciences V. A. Tartakovsky on the occasion of his 90th birthday.

Published in Russian in *Izvestiya Akademii Nauk. Seriya Khimicheskaya,* No. 8, pp. 1604—1613, August, 2022.
1066-5285/22/7108-1604© 2022 Springer Science+Business Media LLC

Diverse physiological processes are controlled by signal molecules, in particular, nitric oxide (NO)[1] involved in cardiovascular tonus modulation, thrombocyte aggregation, immune regulation, nervous system operation, *etc.*[2,3] Nitrosyl iron complexes (NICs) act as depos of NO *in vivo*.[4,5] Their high-molecular-weight protein-bound forms are considered to be most stable and prevail in cells.[6,7] These compounds and their decomposition products are known to actively react with various components of cells and blood plasma (such as heme- and thiol-containing proteins, low-molecular-weight thiols, *etc.*)[4,8,9] and they are also very sensitive to the presence of oxygen in the system.[10—13] It is found[11,14] that oxygen is capable of forming different coordinate bonds in the NICs, which results in diverse reaction routes and a whole set of possible products. An analysis of mechanisms of such transformations would make it possible to evaluate the probability of occurrence of this or another process and to propose structures of the formed products.

The purpose of the present work is the study of the reaction of a promising representative of this class of compounds, *viz.*, NIC with thiourea ligands $[Fe(SC(NH_2)_2)_2(NO)_2]^+$ (complex **1**),[15] with oxygen. Complex **1** in trials *in vitro*, along with the NIC bearing the thiourea derivatives as ligands,[15—18] showed a high cytotoxic and cardiotropic activity, which together with a low toxicity provides a prospect application of this complex for the treatment of socially significant diseases.

Experimental

Materials. 2-Amino-2-hydroxymethypropane-1,3-diol (Tris, Serva, Germany), sulfanyl amide (SA, Sigma—Aldrich, USA), and *N*-(1-naphthyl)ethylenediamine dihydrochloride (NEDA, MP Biomedicals, Germany) were used. Water was distilled in a Bi/Duplex distillator (Germany). The salt of complex **1**, $[Fe(SC(NH_2)_2)_2(NO)_2]Cl \cdot H_2O$, was synthesized as described previously[15] (CIF file CCDC No. 997479).

Operation technique in an inert gas atmosphere was described earlier.[19]

Decomposition of complex 1 under aerobic and anaerobic conditions. Experiments were carried out under anaerobic conditions using a freshly prepared anaerobic solution of complex **1** ($3 \cdot 10^{-3}$ mol L^{-1}) in a 0.05 *M* Tris-HCl buffer (pH 7.0). An aliquot of a solution of the complex was taken and introduced into a 4-mL trial cell with the optical path length 1 cm containing an anaerobic 0.05 *M* Tris-HCl buffer (pH 7.0). The final concentration of complex **1** in a trial cell was $6 \cdot 10^{-5}$ mol L^{-1}.

To prepare aerobic solutions, a weighed sample of complex **1** was dissolved for 5—10 min in a Tris-HCl buffer (pH 7.0) preliminarily purged with oxygen. The final concentration of the complex was (11.8, 20.0, or 41.0) $\cdot 10^{-5}$ mol L^{-1}.

The reference cell contained a 0.05 *M* Tris-HCl buffer (pH 7.0) in all experiments. Absorption spectra were recorded at certain time intervals in the 200—650 nm range at 23 °C on an Agilent Cary 60 spectrophotometer.

Reaction of complex 1 with deoxyhemoglobin (Hb). A homogeneous solution of HbO_2 was isolated from the fresh blood of experimental animals using a standard procedure.[20] To transform HbO_2 into Hb, a 1-mL solution of protein was purged with argon for 10 min. A portion of the prepared solution (200 μL) was introduced into a trial cell containing a 0.05 *M* Tris-HCl buffer (pH 7.0). Then an anaerobic solution of complex **1** with a concentration of $3 \cdot 10^{-3}$ mol L^{-1} was prepared. The reaction was started by introducing 200 μL into a trial cell with Hb. The final concentrations of the complex and protein were $2 \cdot 10^{-4}$ and $2 \cdot 10^{-5}$ mol L^{-1}, respectively. The kinetics of HbNO accumulation was detected for 21 h. To estimate the concentrations of Hb and HbNO, the absorption spectra of the reaction mixture were expanded to components (Hb and HbNO) using the MathCad software as described previously.[19]

Determination of the NO concentration by amperometry. The amount of NO generated by complex **1** in a phosphate buffer (sodium and potassium dihydrophosphates, sodium chloride, phosphoric acid) with pH 6.5 was measured with an amiNO-700 sensor electrode of the inNO measuring system (Innovative Insruments, Inc., USA) for ~500 s (with an increment of 0.2 s). The final concentration of the complex was $44.8 \cdot 10^{-6}$ mol L^{-1}. All experiments were carried out in aerobic 1% aqueous solutions of DMSO at 25 °C and pH 7.0. For the calibration of the electrochemical sensor, a standard aqueous solution of $NaNO_2$ (100 μmol L^{-1}) was used, which was added to a mixture containing KI (20 mg, Aldrich), a 1 *M* solution of H_2SO_4 (2 mL, pure, Khimmed), and water (18 mL).

Determination of the concentration of nitrates using amperometry. The amount of nitrates generated by complex **1** in 50 mL of an aqueous solution containing K_2SO_4 (5 mL, 0.5 mol L^{-1}, VEKTON, Russia) was measured with an Ekom-NO_3 ion-selective electrode of the Ecotest-2000 system (Econix, Russia) in 15 min after the onset of dissolution of the complex. The final concentration of the complex was $6.07 \cdot 10^{-5}$ mol L^{-1}. Standard aqueous solutions of KNO_3 (LenReaktiv, Russia) were used for electrode calibration. To eliminate the influence of nitrite ions, 1% sulfanilic acid (5 mL, LenReaktiv, Russia) was added to the cell.

Determination of the oxygen concentration with oximeter. The oxygen concentration in a solution of complex **1** was measured with an HI 9147 potable oximeter (HANNA Instruments, USA). A weighed sample of complex **1** was dissolved in a 0.05 *M* Tris-HCl buffer (pH 7.0) prepurged with oxygen for 15 min. The final concentrations of complex **1** were (11.7, 21.4, and 40.0) $\cdot 10^{-5}$ mol L^{-1}.

Determination of the concentration of nitrite ions using the Griess test. Solutions of complex **1** with a concentration of $6.07 \cdot 10^{-5}$ mol L^{-1} was prepared in a 0.05 *M* Tris-HCl buffer (pH 7.0). Aliquots of the reaction mixture of complexes (0.3 mL) were sampled and introduced into vessels containing 0.9 mL of a 0.5% solution of SA in 0.25 *M* HCl. After 5 min of incubation, a 0.02% solution of NEDA (0.6 mL) in

0.5 *M* HCl was added. After 10 min, the absorbance at 540 nm was determined. The concentration of nitrites formed by the decomposition of the complex was calculated from the calibration curve plotted for $NaNO_2$.

Quantum chemical calculations were performed with the full geometry optimization of the initial, final, and intermediate complexes in the Gaussian 09 (version D) program[21] using the TPSSh metahybrid functional and 6-311++G**/6-31G* basis set taking into account solvation in an aqueous solution in terms of the polarized continuum model (PCM). Transition states (**TS**) were optimized using the Berny algorithm, and the vibrational frequencies were calculated, which confirmed that these states are saddle points of the first order, since each **TS** has an only imaginary frequency. After the **TS** was found, the resulting wave function was introduced into the calculation of the internal reaction coordinate (IRC) to confirm that the **TS** connects the initial state with the final state. The Born—Oppenheimer molecular dynamics (BOMD) was applied in especially complicated cases where the IRC could not connect two states. In this method, the NVE ensemble was used with the Hartree energy equal to 0.1 (in default), which is characterized by the Boltzmann distribution over all vibrational modes but with the addition of an additional energy value of 50—100 kcal mol^{-1} to the imaginary vibrational mode, and then the calculation was performed. After the analysis of the obtained energy profile, the local maxima as transition states and local minima as intermediate states were optimized using the standard self-consistent field (SCF).

Kinetic modeling. The proposed reaction scheme that describes the processes under study was considered for kinetic modeling. The reaction rate constants were determined by least squares on the basis of numerical solution of the corresponding system of differential equations.

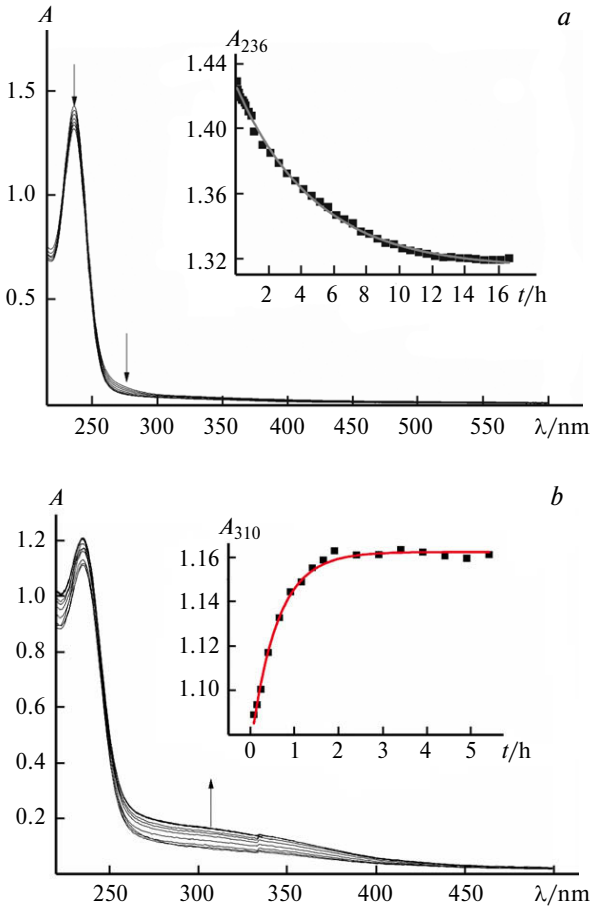

Fig. 1. Change in the absorption spectra of complex **1** under anaerobic (*a*) and aerobic conditions (*b*). Insets: kinetic dependences of changing absorbance at 236 (*a*) and 310 nm (*b*), effective reaction rate constants are $k_{eff} = 5.8 \cdot 10^{-5}$ (*a*) and $4.6 \cdot 10^{-4}$ s^{-1} (*b*). Conditions: initial concentration of complex **1** is $6 \cdot 10^{-5}$ mol L^{-1} (*a*), $4.4 \cdot 10^{-5}$ mol L^{-1} (*b*); Tris-HCl buffer (pH 7.0), 23 °C. Arrows indicate the direction of changing absorbance of the bands in time.

Results and Discussion

*Experimental study of the decomposition of complex **1***

An intense band at 236 nm is observed in the UV spectra of the mononuclear NIC with thiourea ligands (Fig. 1, *a*) as in the earlier studied NICs with the thiourea derivatives.[22,23] No maximum is observed in a range of 250—600 nm in the spectrum of complex **1**, unlike the mononuclear NICs with aliphatic thio ligands characterized[8,24] by the bands at 390 nm. The main band intensity decreases with time, indicating the decomposition of the complex. According to the quantum chemical calculations,[25] this band corresponds to the transfer of an electron from the orbital occupied by lone pairs of the nitrogen atoms of the thiourea ligands (LP(N)) to the unoccupied orbital consisting of d_{z^2}-orbitals of Fe and p-orbitals of S. This means that the decreasing intensity of this maximum is related to the elimination of the thiuourea ligands. The kinetic dependence describing this process reaches a plateau within 14 h (see Fig. 1, *a*, inset).

The shape of the UV spectrum of complex **1** in the presence of oxygen is different (Fig. 1, *b*): the main maximum at 236 nm is retained, but a broad shoulder appears in the 250—400 nm range. Its intensity increases in time, and the curve of the kinetic dependence reaches a plateau within 2 h (see Fig. 1, *b*, inset). The presence of bands in this range is characteristic of a number of the oxygen-containing products.[10] The increase in the absorbance in time observed in the spectra indicates the formation and subsequent transformation of such products.

According to the results obtained on an oximeter, the oxygen concentration decreases in an aqueous solution of complex **1** (Fig. 2). Therefore, a portion of

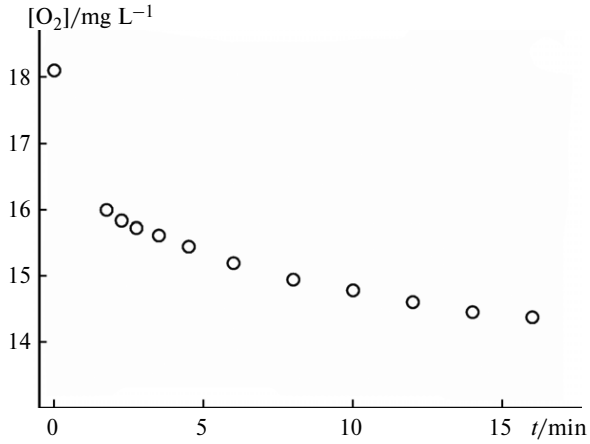

Fig. 2. Oxygen uptake in an aqueous aerobic solution of complex **1**. Conditions: initial concentration of complex **1** is $11.7 \cdot 10^{-5}$ mol L^{-1}; Tris-HCl buffer (pH 7.0), 23 °C.

oxygen is involved in the reaction with the complex, although oxygen can react not only with complex **1** but also with its decay products.

One of the main routes for the reaction of oxygen with the products of decomposition of complex **1** is the oxidation of the formed NO groups. Their generation from the complex and subsequent consumption under aerobic conditions are shown in Fig. 3, *a*. The kinetic curve is bell-shaped, and the maximum is achieved in 90 s. A further decrease in their concentration is related to the formation of nitrites: the major products of the three-step oxidation of NO[26]:

$$4\,NO + O_2 + 2\,H_2O \longrightarrow 4\,NO_2^- + 4\,H^+.$$

Their accumulation in the studied system was examined using the widely known Griess reaction (Fig. 3, *b*).[27] The curve reaches a plateau within the first 15 min of the reaction, and nitrites are accumulated (in the concentration about 6 μmol L^{-1}) within the same time (the concentration of the complex is $6.07 \cdot 10^{-5}$ mol L^{-1}). Note that nitrates are also formed in this system. According to the amperometric results, nitrates are accumulated in a concentration of 24 μmol L^{-1} after the reaction was conducted for 15 min at the same initial concentration of complex **1** in the reaction mixture. The oxidation of nitric oxide to nitrate is known to occur readily in biological media,[28] for example, nitrate is formed stoichiometrically in the reaction of nitric oxide with oxyhemoglobin. In the reaction considered, the oxygen molecule coordinated on hemoglobin is reduced by four electrons, three of which are delivered by nitrogen, and the fourth electron comes from the iron of the heme. This additional reducing equivalent coming from iron makes it possible to change the oxidation state of nitrogen from two to five,

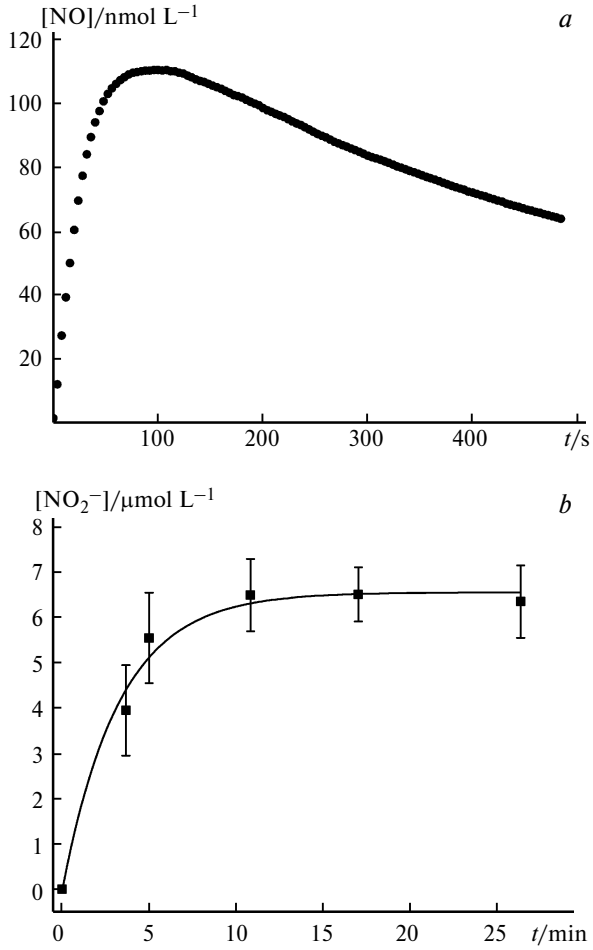

Fig. 3. Kinetic curves of NO generation by complex **1** in aqueous aerobic conditions (*a*) and accumulation of nitrites in an aqueous aerobic solution of complex **1** (*b*). The effective reaction rate constant is $k_{eff} = 5.1 \cdot 10^{-3}$ s^{-1} (*b*). Conditions: initial concentration of complex **1** is $44.8 \cdot 10^{-4}$ mol L^{-1} (*a*), $6.07 \cdot 10^{-5}$ mol L^{-1} (*b*); [Hb] = $2 \cdot 10^{-5}$ mol L^{-1}; phosphate buffer, pH 6.5, 25 °C (*a*), Tris-HCl buffer, pH 7.0, 23 °C (*b*).

i.e., to nitrate formation. In our case, iron of the decayed nitrosyl complex serves as a source of the additional reducing equivalent. In addition, nitrates can be formed due to the hydrolysis of the nitrosyl complex with the ONO_2 ligand, the products of NO_2 coordination at the FeO fragment of the NIC.[11]

When analyzing the decomposition of initial complex **1**, its spontaneous dissociation in aqueous solutions should also be taken into account. In the absence of oxygen, NO is accumulated in this system, but no products observed earlier under the aerobic conditions are formed. To evaluate the NO-donor activity under the anaerobic conditions, we carried out experiments with deoxyhemoglobin (Hb), which is a "trap" of NO (binding constant for the reaction

$$Hb + NO \rightleftharpoons HbNO$$

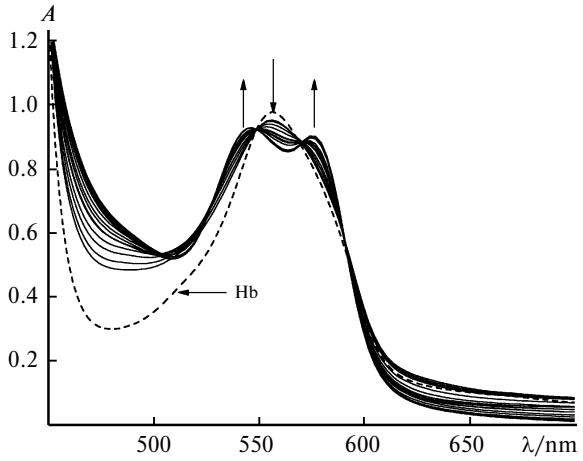

Fig. 4. Change in the absorption spectra for the reaction of complex **1** with Hb. Conditions: initial concentration of complex **1** is $2 \cdot 10^{-4}$ mol L^{-1}; [Hb] = $2 \cdot 10^{-5}$ mol L^{-1}; Tris-HCl buffer, pH 7.0, 23 °C.

is $K = 3 \cdot 10^{10}$ L mol^{-1}).[29] The formed nitrosohemoglobin (HbNO) gives the characteristic spectrum in which one absorption band of Hb (556 nm) is split into two bands (545 and 575 nm) upon the formation of HbNO, and this effect provides a convenient way to determine the reaction depth. The generation of NO from complex **1** is accompanied by the formation of HbNO detected spectrophotometrically as shown in Fig. 4. Unlike the kinetic dependences of accumulation of NO and nitrites formed in air, the accumulation curve of this process reaches a plateau in 6.0—7.5 h after the reaction onset (Fig. 5), which corresponds to the complete saturation of the protein with NO.

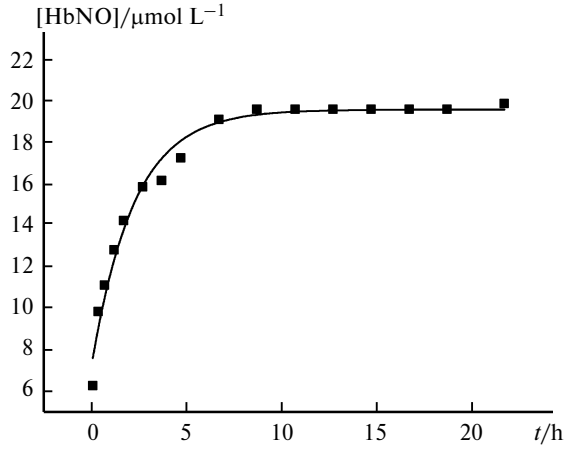

Fig. 5. Kinetic curve of HbNO accumulation in the reaction of complex **1** with Hb under aerobic conditions. The effective reaction rate constant is $k_{eff} = 1.2 \cdot 10^{-4}$ s^{-1}. Conditions: initial concentration of complex **1** is $2 \cdot 10^{-4}$ mol L^{-1}; [Hb] = $= 2 \cdot 10^{-5}$ mol L^{-1}; Tris-HCl buffer, pH 7.0, 23 °C.

Thus, according to the experimental data, complex **1** actively reacts with oxygen to form various oxygen-containing products. Under anaerobic conditions, the complex decomposes to form NO and thiourea ligands.

*Kinetic and quantum chemical modeling of the decomposition of complex **1** under aerobic conditions*

The kinetic modeling method was applied to study the transformation mechanism of complex **1** under aerobic conditions in more detail. According to the previous results,[10] complex **1** can interact with an oxygen molecule *via* different routes to form a number of products.

A sharp decrease in the [O_2] concentration at the initial moment upon the introduction of complex **1** into the system is observed on the experimental curves of oxygen uptake (Fig. 6). This can be explained by the reversible reaction for which the equilibrium condition (so-called detailed equilibrium) is hold at every moment, including the initial moment:

$$\mathbf{1} + O_2 \overset{K_0}{\rightleftharpoons} \mathbf{1}O_2, \qquad (1)$$

where $\mathbf{1}O_2$ is the product of oxygen molecule coordination on complex **1**, and K_0 is the equilibrium constant.

To describe this process, we obtained the optimized geometries for three possible coordination modes of oxygen (Fig. 7) to which complexes **2**—**4** correspond. An oxygen molecule can attack a molecule of initial complex **1** at the Fe atom (complex **2**), Fe—N bond (complex **3**), or two N atoms of the nitrosyl groups (complex **4**).

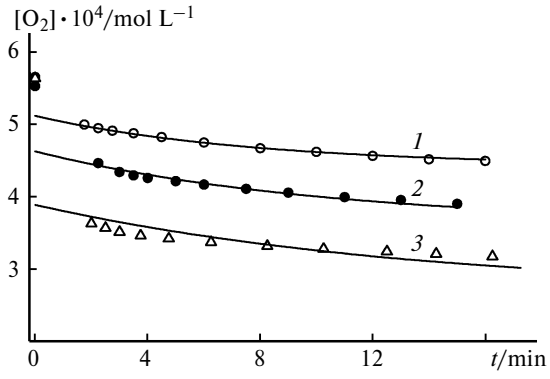

Fig. 6. Kinetic curves of the oxygen uptake in the presence of complex **1**. Conditions: initial concentrations of the complex are $[\mathbf{1}]_0 \cdot 10^5 = 11.7$ (*1*), 21.4 (*2*), and 40.0 mol L^{-1} (*3*); initial oxygen concentrations are $[O_2]_0 \cdot 10^5 = 55.8$ (*1*), 54.1 (*2*), and 58.2 mol L^{-1} (*3*); Tris-HCl buffer, pH 7.0, 23 °C; points are experiment; and lines are calculation from the determined kinetic parameters.

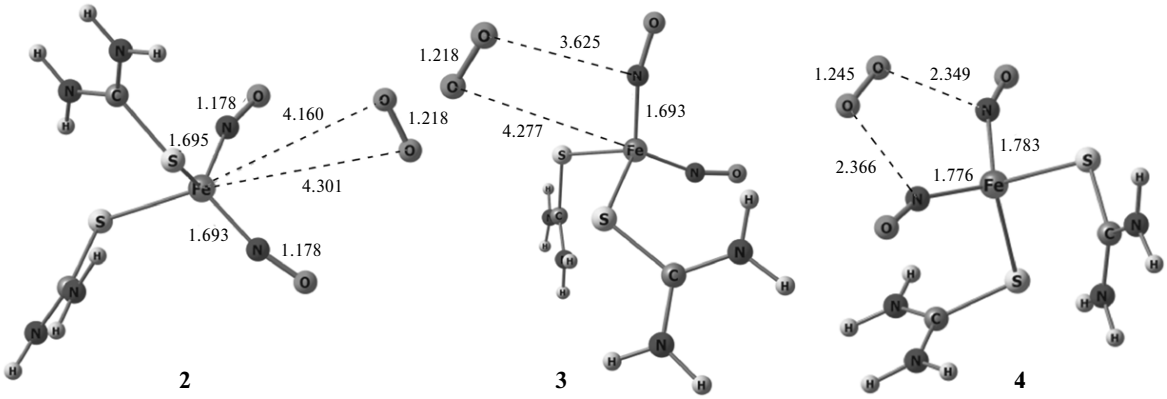

Fig. 7. Optimized geometries of molecular complexes **2**—**4** corresponding to $\mathbf{1}O_2$ in Eq. (1); interatomic distances are given (Å).

In addition, when analyzing the complex **1**—oxygen reaction system, one should consider the spontaneous transformation of the complex

$$\mathbf{1} \xrightarrow{k_1} P_1, \qquad (2)$$

where P_1 is the transformation products.

As shown previously,[30] the initial complex can decompose with the cleavage of the Fe—N and Fe—S bonds. According to the calculation (AIM and NBO) results, the strength of the bond between the thiourea ligand and the Fe atom is two times smaller than that of Fe with the NO ligand. The formed tricoordinate iron products are unstable and can react with solvent molecules or undergo dimerization. The experimentally observed decrease in the absorbance in time under anaerobic conditions (see Fig. 1, *a*), which indicates thio ligand elimination, and the accumulation of NO (see Fig. 5) confirm the earlier quantum chemical modeling data on the cleavage of the Fe—N and Fe—S bonds during the transformation of complex **1**.

The third route in the analyzed system results in the formation of products of the reaction of the complex with an oxygen molecule:

$$\mathbf{1} + O_2 \xrightarrow{k_2} Q, \qquad (3)$$

where Q is a set of the products of the reaction of complex **1** with oxygen, whose formation changes the absorbance of the system. We succeeded in calculating three possible routes of reaction (3) depending on the way in which oxygen attacks a molecule of complex **1**.

In the case where oxygen directly attacks the Fe atom of complex **1**, the further formation of complex **1a** can be envisaged (Fig. 8, *a*). The process requires an energy expense of 14.2 kcal mol^{-1}, and formed complex **1a** represents a hexacoordinate iron complex with the O_2 ligand. Note that one Fe—NO bond in this complex lengthens by 0.25 Å compared to the optimized geometry of the initial complex.[10] It can be expected that this ligand could readily be eliminated, since the energy needed for this reaction, according to our calculations, is only 3.1 kcal mol^{-1}. In addition, this reaction can be reversible and NO can add to product **1a**. According to our calculations, the process can also occur further; *i.e.*, complex **1b** can also transform *via* two different routes with different transition states. Although both routes include the O—O bond cleavage, the pentacoordinate iron complex with a very weak Fe—NO bond (complex **1c**) is formed in the first case, whereas oxygen is inserted at the Fe—S bond with the formation of the mononitrosyl iron complex with the $OSC(NH_2)_2$ ligand (complex **1d**) in the second case; *i.e.*, intramolecular oxidation occurs. Then NO can detach itself from complex **1c** to form complex **1e**, which is associated with an energy barrier of 6.4 kcal mol^{-1} only. The backward process can be assumed, namely, the addition of NO to compound **1e** with the formation of compound **1f**, which would occur with a significant energy gain (21.0 kcal mol^{-1}). At the same time, although the intramolecular oxidation itself is exothermal in the case Fe—S, this process is characterized by a high activation barrier and would be reversible with a low probability.

The second route assumed for the reaction of complex **1** with oxygen (at the Fe—N bond) leads to the formation of complex **2a**, which gives complex **2b** with the NO_2, NO, and O ligands *via* a low energy barrier of the O—O bond cleavage. Since the intramolecular oxidation of the Fe—S bond occurs simultaneously, complex **2c** lying at a lower energy level (Fig. 8, *b*) can be formed. On the contrary, complex **2b** undergoes the further transformation associated with either the reversible elimination (complex **2d**) and addition of NO_2 (complex **2f**), or oxidation of the NO ligand to NO_2

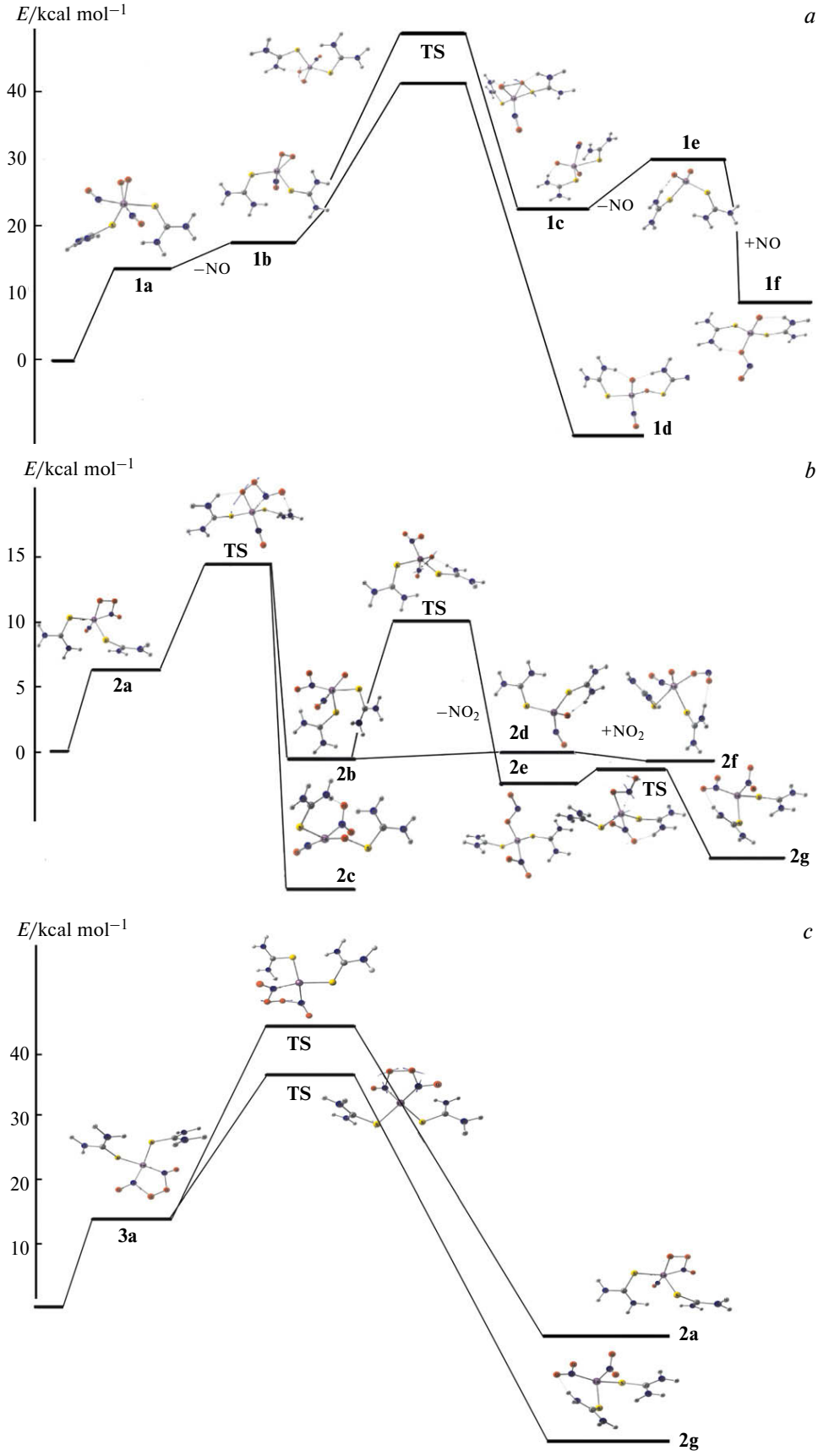

Fig. 8. Energy profiles of the reactions of complex **1** with oxygen: coordination at the iron atom (*a*), Fe—N bond (*b*), and nitrogen atoms of the NO ligands (*c*).

(complex **2g**), which is accompanied by the known nitro-nitrite rearrangement.[31] On the whole, all reactions of this route (see Fig. 8, *b*) can be reversible, except for the formation of complexes **2c** and **2g**.

The third route involving two nitrogen atoms of the NO groups results in complex **3a** capable of decomposing to form either stable complex **2g**, or complex **2a** again (Fig. 8, *c*). Thus, in this case, the reaction would proceed *via* the second route (see Fig. 8, *b*), but insignificant energy barriers, which are especially pronounced for the backward reactions, make the equilibrium impossible. Thus, the experimentally observed (see Fig. 1, *b*) change in the absorbance is related to the formation of a set of products presented in Fig. 8. Since an exact composition of the products is unknown, we characterized them by the overall molar absorption coefficient ε. The kinetic curves on the initial region of the process, where the absorbance increases due to the formation of products Q, are shown in Fig. 9.

As can be seen from the data in Fig. 10, when the absorbance achieves the highest value it decreases then slightly to reach a constant (different from zero) value. This behavior of the experimental data can be explained by the reversible consumption of products Q with the rate constants k_3 and k_{-3}:

$$Q \underset{k_{-3}}{\overset{k_3}{\rightleftharpoons}} P_2. \qquad (4)$$

The system of equations corresponding to the scheme of reactions (1)—(4) with an allowance for detailed equilibrium in reaction (1) has the following form:

$$d[\mathbf{1}]/dt = -(k_1[\mathbf{1}](1 + K_0[\mathbf{1}]) + k_2[\mathbf{1}][O_2])/B(t), \qquad (I)$$

$$d[O_2]/dt = (k_1[\mathbf{1}]K_0[O_2] - k_2[\mathbf{1}][O_2])/B(t), \qquad (II)$$

$$d[Q]/dt = k_2[\mathbf{1}][O_2] - k_3[Q] + k_{-3}[P_2], \qquad (III)$$

$$d[P_2]/dt = k_3[Q] - k_{-3}[P_2], \qquad (IV)$$

$$d[P_1]/dt = k_1[\mathbf{1}]; \qquad (V)$$

the initial conditions with an allowance for the equilibrium character of reaction (1) are as follows:

$$[\mathbf{1}](0) = [-(1 + c_0) + (1 + c_0^2 + 2d_0)^{0.5}]/(2K_0),$$

$$[O_2](0) = [-(1 - c_0) + (1 + c_0^2 + 2d_0)^{0.5}]/(2K_0),$$

$$[Q](0) = [P_1](0) = [P_2](0) = 0,$$

where $B(t) = 1 + K_0[\mathbf{1}] + K_0[O_2]$; $c_0 = K_0([O_2]_0 - [\mathbf{1}]_0)$; $d_0 = K_0([O_2]_0 + [\mathbf{1}]_0)$; $[\mathbf{1}]_0$ and $[O_2]_0$ are the initial concentrations of complex **1** and oxygen in the system.

The absorbance of the system measured in experiment was $A(t) = \varepsilon[Q]$. The main task was to calculate the equilibrium constant K_0 using experimental data (see Figs 6, 9, and 10), as well as the reaction rate constants k_1, k_2, k_3, and k_{-3} and molar absorption coefficient ε.

The equilibrium constant K_0 and rate constants k_1 and k_2 can be determined following the oxygen uptake in the system. For this purpose, the equilibrium oxygen

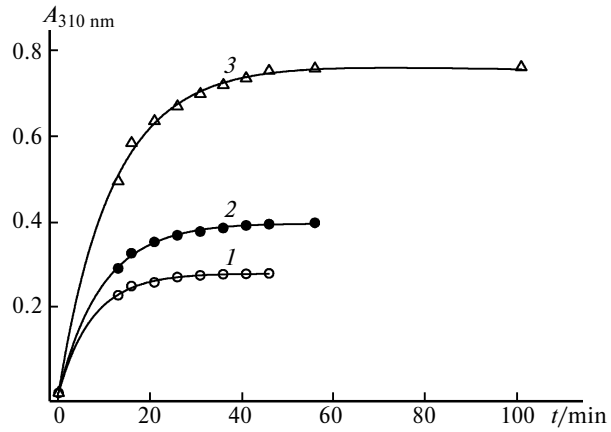

Fig. 9. Initial regions of the kinetic curves of changing absorbance for the complex **1**—oxygen system. Conditions: initial concentrations of the complex are $[\mathbf{1}]_0 \cdot 10^5$ = 11.8 (*1*), 20.0 (*2*), and 41.0 mol L^{-1} (*3*); initial oxygen concentrations are $[O_2]_0 \cdot 10^5$ = = 56.5 (*1*), 55.3 (*2*), and 56.4 mol L^{-1} (*3*); Tris-HCl buffer, pH 7.0, 23 °C; points are experiment; and lines are calculation from the determined kinetic parameters.

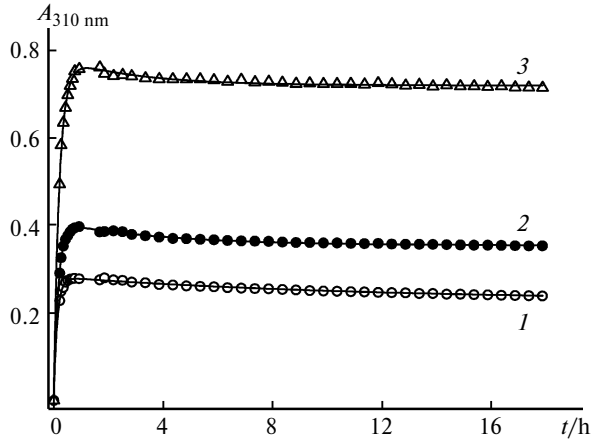

Fig. 10. Kinetic curves of changing absorbance for the complex **1**—oxygen system. Conditions: initial concentrations of the complex are $[\mathbf{1}]_0 \cdot 10^5$ = 11.8 (*1*), 20.0 (*2*), and 41.0 mol L^{-1} (*3*); initial oxygen concentrations are $[O_2]_0 \cdot 10^5$ = 56.5 (*1*), 55.3 (*2*), and 56.4 mol L^{-1} (*3*); Tris-HCl buffer, pH 7.0, 23 °C; points are experiment; and lines are calculation from the determined kinetic parameters.

Table 1. Kinetic parameters of the reaction of complex **1** with oxygen

$[\mathbf{1}]_0 \cdot 10^5$	$[O_2]_0 \cdot 10^5$	$K_0 \cdot 10^{-3}$	$k_1 \cdot 10^4/s^{-1}$	k_2/L mol^{-1}	$k_3 \cdot 10^6$	$k_{-3} \cdot 10^5$	$\varepsilon \cdot 10^{-3}$
mol L^{-1}		/L mol^{-1}			s^{-1}		/L mol^{-1} cm^{-1}
11.8	56.5	1.27	<1	7.2	4.7	2.0	2.41
20.0	55.3	1.25	3.7	5.0	8.8	6.1	2.38
41.0	56.4	2.41	5.0	5.7	7.7	9.1	2.45

concentration $[O_2](0)$ at the initial moment was first determined by the extrapolation of the experimental $[O_2](t)$ values on the basis of each curve presented in Fig. 6, and K_0 was found using this concentration. Then the k_1 and k_2 constants were determined using the $[O_2](t)$ dependence by the minimization of the functional

$$\Phi(k_1 k_2) = \sum_{j=1}^{n} \left\{ [O_2]_{exp}(t_j) - [O_2]_{calc}(t_j) \right\}^2,$$

being the sum of squared deviations at specified moments t_j of the calculated $[O_2]_{calc}(t_j)$ and experimental $[O_2]_{exp}(t_j)$ oxygen concentrations $[O_2](t)$.

Then the kinetics of accumulation of products Q in the corresponding experiments (see Fig. 9) was calculated using the determined parameters, and the molar absorption coefficient ε was determined and the k_1 and k_2 constants were refined by comparing the calculated and experimental values. Taking into account the final (after the maximum) region of the time dependence of the absorbance (see Fig. 10), we estimated the rate constants k_3 and k_{-3}. The calculation results are given in Table 1. The calculated and experimental kinetic curves are compared in Figs 6, 9, and 10.

The scheme of reactions (1)—(4) with the determined parameters satisfactorily describe the experimental data.

To conclude, the mechanism of the decomposition of the nitrosyl iron complex with thiourea ligands (complex **1**) under aqueous aerobic conditions was examined on the basis of the experimental data obtained using the kinetic and quantum chemical modeling. The presence of oxygen in the system substantially affects possible routes of the reaction of complex **1** under these conditions. The obtained data indicate that oxygen coordinates to different positions in the structure of complex **1**, which further results in the oxidation of the ligands. The process is accompanied by an oxygen uptake in the reaction mixture and the appearance of a broad shoulder in a range of 250—400 nm in the absorption spectrum. The rate constants (see Table 1) found by kinetic modeling satisfactorily describe the obtained experimental data.

The specific features found for the decomposition of nitrosyl complex **1** under aerobic conditions should be taken into account in the further modeling and studying the mechanisms of its reactions with targets *in vitro* and *in vivo*.

This work was carried out in terms of state assignment (state registration Nos AAAA-A19-119071890015-6 and AAAA-A19-119111390022-2).

No human or animal subjects were used in this research.

The authors declare no competing interests.

References

1. N. S. Bryan, D. J. Lefer, *Mol. Pharmacol.*, 2019, **96**, 109; DOI: 10.1124/mol.118.113910.
2. L. J. Ignarro, *J. Physiol. Pharmacol.*, 2002, **53**, 503.
3. S. Korde Choudhari, M. Chaudhary, S. Bagde, A. R. Gadbail, V. Joshi, *World J. Surg. Oncol.*, 2013, **11**, 118; DOI: 10.1186/1477-7819-11-118.
4. N. Lehnert, E. Kim, H. T. Dong, J. B. Harland, A. P. Hunt, E. C. Manickas, K. M. Oakley, J. Pham, G. C. Reed, V. S. Alfaro, *Chem. Rev.*, 2021, **121**, 14682; DOI: 10.1021/acs.chemrev.1c00253.
5. C.-Y. Chiang, M. Y. Darensbourg, *J. Biol. Inorg. Chem.*, 2006, **11**, 359; DOI: 10.1007/s00775-006-0084-y.
6. A. F. Vanin, S. V. Kiladze, L. N. Kubrina, *Biofizika* [*Biophysics*], 1975, **20**, 1068—1072 (in Russian).
7. T. Ueno, T. Yoshimura, *Jpn J. Pharmacol.*, 2000, **82**, 95; DOI: 10.1254/jjp.82.95.
8. H. Lewandowska, M. Kalinowska, K. Brzóska, K. Wójciuk, G. Wójciuk, M. Kruszewski, *Dalton Trans.*, 2011, **40**, 8273; DOI: 10.1039/C0DT01244K.
9. N. I. Neshev, E. M. Sokolova, G. I. Kozub, T. A. Kondrat´eva, N. A. Sanina, *Russ. Chem. Bull.*, 2020, **69**, 1987; DOI: 10.1007/s11172-020-2989-y.
10. N. S. Emel´yanova, L. G. Gutsev, O. V. Pokidova, A. F. Shestakov, N. A. Sanina, S. M. Aldoshin, *Inorg. Chim. Acta*, 2021, **522**, 120361; DOI: 10.1016/j.ica.2021.120361.
11. A. Banerjee, S. Sen, A. Paul, *Chem. — A Eur. J.*, 2018, **24**, 3330; DOI: 10.1002/chem.201705726.
12. O. V. Pokidova, N. S. Emel´yanova, B. L. Psikha, A. V. Kulikov, B. A. Tretyakov, A. I. Kotel´nikov, N. A. Sanina, S. M. Aldoshin, *Inorg. Chim. Acta*, 2020, **502**, 119369; DOI: 10.1016/j.ica.2019.119369.

13. H. L. K. Wah, M. Postel, F. Tomi, *Inorg. Chem.*, 1989, **28**, 233; DOI: 10.1021/ic00301a015.
14. N. A. Sanina, N. S. Emel´yanova, A. N. Chekhlov, A. F. Shestakov, I. V. Sulimenkov, S. M. Aldoshin, *Russ. Chem. Bull.*, 2010, **59**, 1126; DOI: 10.1007/s11172-010-0215-z.
15. N. A. Sanina, S. M. Aldoshin, N. Y. Shmatko, D. V. Korchagin, G. V. Shilov, N. S. Ovanesyan, A. V. Kulikov, *Inorg. Chem. Commun.*, 2014, **49**, 44; DOI: 10.1016/j.inoche.2014.09.016.
16. N. A. Sanina, N. Y. Shmatko, D. V. Korchagin, G. V. Shilov, A. A. Terent´ev, T. S. Stupina, A. A. Balakina, N. V. Komleva, N. S. Ovanesyan, A. V. Kulikov, S. M. Aldoshin, *J. Coord. Chem.*, 2016, **69**, 812; DOI: 10.1080/00958972.2016.1142536.
17. N. Sanina, N. Shmatko, T. Stupina, A. Balakina, A. Terent´ev, *Molecules*, 2017, **22**, 1426; DOI: 10.3390/molecules22091426.
18. V. M. Ignat´ev, N. S. Emel´yanova, N. A. Sanina, *Russ. Chem. Bull.*, 2020, **69**, 2265; DOI: 10.1007/s11172-020-3045-7.
19. N. A. Sanina, L. A. Syrtsova, N. I. Shkondina, T. N. Rudneva, E. S. Malkova, T. A. Bazanov, A. I. Kotel´nikov, S. M. Aldoshin, *Nitric Oxide*, 2007, **16**, 181; DOI: 10.1016/j.niox.2006.10.005.
20. G. Geraci, L. J. Parkhurst, Q. H. Gibson, *J. Biol. Chem.*, 1969, **244**, 4664; DOI: 10.1016/S0021-9258(18)93675-6.
21. M. J. Frisch, G. W. Trucks, H. B. Schlegel, G. E. Scuseria, M. A. Robb, J. R. Cheeseman, G. Scalmani, V. Barone, B. Mennucci, G. A. Petersson, H. Nakatsuji, M. Caricato, X. Li, H. P. Hratchian, F. Izmaylov, J. Bloino, G. Zheng, J. L. Sonnenberg, M. Hada, M. Ehara, K. Toyota, R. Fukuda, J. Hasegawa, M. Ishida, T. Nakajima, Y. Honda, O. Kitao, H. Nakai, T. Vreven, J. A. Montgomery, Jr., J. E. Peralta, F. Ogliaro, M. Bearpark, J. J. Heyd, E. Brothers, K. N. Kudin, V. N. Staroverov, T. Keith, R. Kobayashi, J. Normand, K. Raghavachari, A. Rendell, J. C. Burant, S. S. Iyengar, J. Tomasi, M. Cossi, N. Rega, J. M. Millam, M. Klene, J. E. Knox, J. B. Cross, V. Bakken, C. Adamo, J. Jaramillo, R. Gomperts, R. E. Stratmann, O. Yazyev, A. J. Austin, R. Cammi, C. Pomelli, J. W. Ochterski, R. L. Martin, K. Morokuma, V. G. Zakrzewski, G. A. Voth, P. Salvador, J. J. Dannenberg, S. Dapprich, A. D. Daniels, O. Farkas, J. B. Foresman, J. V. Ortiz, J. Cioslowski, D. J. Fox, *GAUSSIAN 09*, Revision D.01, Gaussian, Inc., Wallingford (CT), 2013.
22. O. V. Pokidova, N. S. Emel´yanova, A. Y. Kormukhina, V. O. Novikova, A. V. Kulikov, A. I. Kotelnikov, N. A. Sanina, *Dalton Trans.*, 2022, **51**, 6473; DOI: 10.1039/d2dt00291d.
23. O. V. Pokidova, A. Y. Kormukhina, A. I. Kotelnikov, T. N. Rudneva, K. A. Lyssenko, N. A. Sanina, *Inorg. Chim. Acta*, 2021, **524**, 120453; DOI: 10.1016/j.ica.2021.120453.
24. A. F. Vanin, A. P. Poltorakov, V. D. Mikoyan, L. N. Kubrina, D. S. Burbaev, *Nitric Oxide*, 2010, **23**, 136; DOI: 10.1016/j.niox.2010.05.285.
25. O. V. Pokidova, N. S. Emel´yanova, B. L. Psikha, N. A. Sanina, A. V. Kulikov, A. I. Kotel´nikov, S. M. Aldoshin, *J. Mol. Struct.*, 2019, **1192**, 264; DOI: 10.1016/j.molstruc.2019.05.005.
26. L. J. Ignarro, J. M. Fukuto, J. M. Griscavage, N. E. Rogers, R. E. Byrns, *Proc. Natl. Acad. Sci.*, 1993, **90**, 8103; DOI: 10.1073/pnas.90.17.8103.
27. M. N. Möller, N. Rios, M. Trujillo, R. Radi, A. Denicola, B. Alvarez, *J. Biol. Chem.*, 2019, **294**, 14776; DOI: 10.1074/jbc.REV119.006136.
28. C. Helms, D. B. Kim-Shapiro, *Free Radic. Biol. Med.*, 2013, **61**, 464; DOI: 10.1016/j.freeradbiomed.2013.04.028.
29. E. Antonini, M. Brunori, in *North-Holland Research Monographs. Frontiers of Biology*, Eds E. L. Tatum, A. Neuberger, North-Holland Publishing Company, Amsterdam—London, 1971, Vol. **21**, p. 276.
30. N. S. Emel´yanova, N. Yu. Shmatko, N. A. Sanina, S. M. Aldoshin, *Russ. Chem. Bull.*, 2017, **66**, 1842; DOI: 10.1007/s11172-017-1955-9.
31. D. Ampadu Boateng, M. D. Word, L. G. Gutsev, P. Jena, K. M. Tibbetts, *J. Phys. Chem. A*, 2019, **123**, 1140; DOI: 10.1021/acs.jpca.8b11723.

Received April 29, 2022;
in revised form June 20, 2022;
accepted June 21, 2022